ISSN 1027-4510, Journal of Surface Investigation: X-ray, Synchrotron and Neutron Techniques, 2023, Vol. 17, No. 2, pp. 494–499. © Pleiades Publishing, Ltd., 2023.
Russian Text © The Author(s), 2023, published in Poverkhnost', 2023, No. 4, pp. 101–106.

# Composition and Structure of fcc-Structured High-Entropy Alloys Irradiated with Helium Ions

**V. V. Uglov[a, *], I. A. Ivanov[b], S. V. Zlotski[a], N. A. Stepanjuk[a], A. E. Ryskulov[b], A. L. Kozlovski[b], A. E. Kurahmedov[b], M. V. Koloberdin[b], A. D. Sapar[b], E. O. Ungarbaev[b], and K. Jin[c]**

[a] *Belarusian State University, Minsk, 220030 Belarus*

[b] *Nuclear Physics Institute, Ministry of Energy of the Republic of Kazakhstan, Astana, 010008 Kazakhstan*

[c] *Beijing Institute of Technology, Beijing, 100811 China*

**e-mail: uglov@bsu.by*

Received July 14, 2022; revised September 28, 2022; accepted September 28, 2022

**Abstract**—Bulk samples of CoCrFeNi and CoCrFeMnNi high-entropy alloys, prepared by arc melting from a powder of a purity up to 99.97% under an argon atmosphere followed by annealing (1150°C, 24 and 72 h) and cold rolling (85% reduction in thickness), are irradiated with $He^{2+}$ ions (energy of 40 keV, f luence of $2 \times 10^{17}$ $cm^{-2}$). CoCrFeNi and CoCrFeMnNi samples are substitutional solid solutions with a composition close to equiatomic and a uniform distribution of elements over the depth of the alloys. They have a coarse grain structure with a grain size of about 80 μm for CoCrFeNi and 100 μm for CoCrFeMnNi. The surface microstructure and the phase and elemental composition of high-entropy alloys are resistant to irradiation. No traces of radiation erosion or changes in the elemental and phase composition of the alloys are found. In alloys, the dislocation density increases, which leads to a decrease in the size of the coherent-scattering regions, and helium bubbles are also formed, leading to an increase in compressive macrostress. Tensile microstress prevails in irradiated CoCrFeNi alloys, while compressive stress prevails in CoCrFeMnNi alloys. High-entropy CoCrFeMnNi alloys with a more complex composition are more resistant to radiation damage.

**Keywords:** high-entropy alloys, ion irradiation, radiation-defect formation, microstress, macrostress, X-ray phase analysis

**DOI:** 10.1134/S1027451023020398

## INTRODUCTION

Modern challenges facing the scientific and technological side of nuclear power are concentrated around improving the efficiency of nuclear power plants by increasing their operating temperatures [1–3]. Conventional materials, such as austenitic steels, nickel, and other metal alloys with a base of one or two elements, undergo phase transformations and the decomposition of solid solutions at elevated temperatures, corrode upon contact with liquid coolants and many gases, and swell at high doses of neutron irradiation [2, 3]. Under such conditions, they are prone to embrittlement and loss of operating properties. A solution to these problems requires the development of new materials, since the current structural materials of nuclear installations are not capable of long-term operation in chemically aggressive environments at elevated temperatures. Achieving this goal will also give impetus to the development of jet power plants and elements of aerospace vehicles [1–4].

High-entropy alloys (HEAs) are among the most promising classes of materials for solving such problems [1–7]. They attract the attention of scientists from all over the world, and the studies of the teams led by Cantor and Senkov are recognized as pioneers in this field [8, 9].

HEAs have a structure different from most of the known homogeneous alloys: it cannot always be represented as a solid-solution lattice based on the lattice of one element due to high disorder in this structure [1, 7]. The increased entropy of mixing elements contributes to minimizing the value of the Gibbs free energy and, thus, increasing the thermodynamic stability of the HEA. Considering the variety of types of solid solutions that can be created, theoretically, HEA-type materials can have any properties [10, 11].

It is also worth noting the so-called “recovery effect” in HEAs, which is mentioned in many works on the radiation resistance of these alloys [12, 15]. This effect implies the possibility of returning the lattice to its original state (before irradiation) in samples irradiated with ions by neutralizing radiation-induced defects. For example, by selecting the proper operating temperature, it is possible to achieve permanent restoration of the HEA structure during irradiation using

**Table 1.** Elemental composition of CoCrFeNi and CoCrFeMnNi HEAs not irradiated (n/i) and irradiated with $He^{2+}$ ions (40 keV, $2 \times 10^{17}$ $cm^{-2}$)

| Sample | Element concentration, at % | | | | |
|---|---|---|---|---|---|
| | Co | Cr | Fe | Ni | Mn |
| CoCrFeNi (n/i) | 24.8 ± 0.1 | 25.8 ± 0.1 | 25.0 ± 0.1 | 24.4 ± 0.1 | – |
| CoCrFeNi ($He^{2+}$) | 24.6 ± 0.3 | 25.5 ± 0.3 | 25.5 ± 0.3 | 24.4 ± 0.3 | – |
| CoCrFeMnNi (n/i) | 20.7 ± 0.2 | 18.9 ± 0.1 | 20.0 ± 0.2 | 20.4 ± 0.2 | 20.0 ± 0.1 |
| CoCrFeMnNi ($He^{2+}$) | 19.6 ± 0.2 | 20.5 ± 0.2 | 19.8 ± 0.2 | 20.8 ± 0.2 | 19.5 ± 0.2 |

the "self-healing effect" directly during operation [12–17].

All of the above makes HEAs promising materials for nuclear power plants and aircraft power units [15–19].

HEAs can be divided into three main groups: based on 3*d* transition metals, based on refractory metals, and based on rare-earth elements. The first two groups of alloys are the most economically justified and, therefore, the most frequently considered [20]. Nickel-containing HEAs with a face-centered cubic structure show increased radiation resistance in comparison with steels and nickel supermetals of the Inconel type [6]. The reasons for such behavior of nickel-containing HEAs still do not have an accurate explanation or description, aided by conf licting data on their properties and likely operating capabilities.

The purpose of this work is to study the radiation resistance of CoCrFeNi and CoCrFeMnNi high-entropy alloys and the mechanisms of the behavior of defects under irradiation with α particles.

## EXPERIMENTAL

Samples of CoCrFeNi and CoCrFeMnNi alloys were obtained at the Beijing Institute of Technology (China) using the following technology. Bulk ingots were prepared from powders of pure (up to 99.97%) metals by arc melting under high-purity argon, followed by casting into copper cuvettes. After crystallization, the ingots were annealed for 24 h at 1150°C to spheroidize and homogenize the grain structure of the samples. Subsequently, cold rolling was carried out until the thickness of the ingots decreased by 85%, and final annealing at 1150°C was carried out for 72 h to smooth the texture and decrease the stress caused by rolling.

All samples had the shape of rectangular parallelepipeds with linear dimensions of 5.0 × 5.0 × 1.5 mm.

The samples were irradiated at a DTs-60 ion accelerator at the Astana Branch of the Institute of Nuclear Physics (Kazakhstan), using $He^{2+}$ ions with an energy of 40 keV at a f luence of $2 \times 10^{17}$ $cm^{-2}$. This type of ions arises due to the interaction of neutrons with atoms of matter, followed by alpha decay, which leads to the formation of gas bubbles, areas of increased internal stress, accumulation of helium in the material, and, as a result, its swelling.

The surface morphology and elemental composition of the samples were analyzed by scanning electron microscopy (SEM) and energy-dispersive X-ray spectrometry using a ZEISS LEO 1455 VP scanning electron microscope; the images were obtained at an accelerating voltage of 20 kV.

The elemental composition and depth distribution of elements were studied by the Rutherford-backscattering method on a DTs-60 setup using $N^{2+}$ ions with an energy of 14 MeV.

Phase analysis of the samples was carried out by X-ray diffraction (X-ray phase analysis). The X-ray diffraction patterns were obtained using a Rigaku Ultima IV X-ray diffractometer in the parallel-beam geometry using Cu$K_\alpha$ characteristic X-ray radiation with a wavelength of $\lambda$ = 0.154179 nm. The measurements were carried out at a constant rotation of the samples at a speed of 30 rps to eliminate the effect of the texture of the alloys.

## RESULTS

The results of studying the elemental composition of CoCrFeNi and CoCrFeMnNi alloys are given in Table 1. According to these data, the composition of the alloys is close to equiatomic. Rutherford backscattering confirmed the equiatomic composition of the samples and revealed a uniform distribution of elements over the depth of the alloys.

Investigation of the elemental composition of the samples after irradiation with $He^{2+}$ ions did not reveal its noticeable deviation from the initial composition. Rutherford backscattering also showed no changes in the homogeneous distribution of elements over depth. The distribution of elements is not observed precisely in the surface layer, in which helium implantation occurs.

The results of SEM studies of CoCrFeNi and CoCrFeMnNi samples are shown in Figs. 1 and 2, respectively. The alloys have a coarse-grained structure with a grain size of about 80 μm for CoCrFeNi and 100 μm for CoCrFeMnNi (Figs. 1a and 2a). In all samples, the grains have a regular polygonal shape

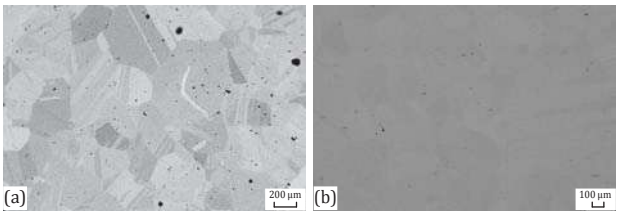


**Fig. 1.** SEM image of the surface of the (a) initial CoCrFeNi alloy and (b) that irradiated with $He^{2+}$ ions (40 keV, $2 \times 10^{17}$ $cm^{-2}$).

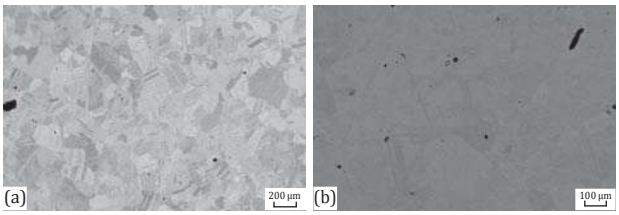


**Fig. 2.** SEM image of the surface of the (a) initial CoCrFeMnNi alloy and (b) that irradiated with $He^{2+}$ ions (40 keV, $2 \times 10^{17}$ $cm^{-2}$).

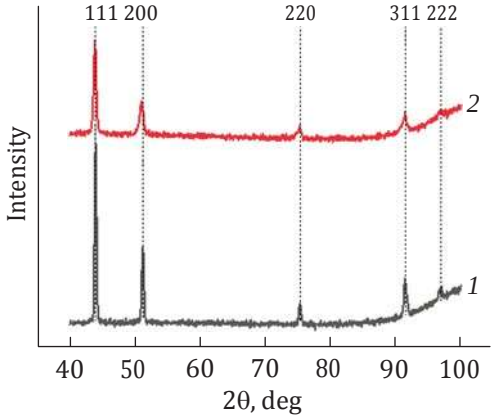


**Fig. 3.** X-ray diffraction patterns of CoCrFeNi alloy samples (*1*) not irradiated and (*2*) irradiated with $He^{2+}$ ions (40 keV, $2 \times 10^{17}$ $cm^{-2}$); the numbers show the reflection indices.

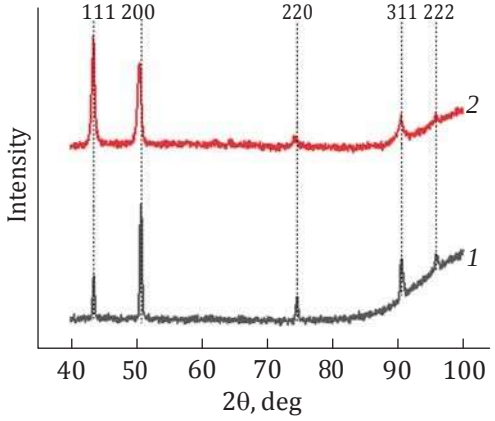


**Fig. 4.** X-ray diffraction patterns of CoCrFeMnNi alloy samples (*1*) not irradiated and (*2*) irradiated with $He^{2+}$ ions (40 keV, $2 \times 10^{17}$ $cm^{-2}$); the numbers show the reflection indices.

with traces of twinning introduced by cold rolling. After irradiation with helium ions, the surface morphology of the samples is preserved (Figs. 1b and 2b). No traces of surface erosion are noticeable, which confirms the resistance of their surface structure to irradiation with helium ions.

The results of phase analysis of the initial and $He^{2+}$-irradiated HEAs are shown in Figs. 3 and 4. The X-ray patterns were obtained at a small angle of incidence of radiation on the sample ($\alpha = 1°$), which corresponds to an X-ray penetration depth of about 300 nm. This depth, according to SRIM calculations [21], corresponds to the range of helium ions with an energy of 40 keV.

Analysis of the X-ray diffraction patterns (Figs. 3 and 4) showed that these HEAs are single-phase systems with a fcc lattice.

Analysis of the formed phases and comparison of the angular positions of their diffraction reflections with the peaks from pure fcc metals included in the composition of the alloys showed that the HEA peaks are located between the corresponding peaks of pure metals, which indicates the formation of substitutional solid solutions. The lattice period calculated from X-ray diffraction patterns for the CoCrFeNi alloy was $0.3585 \pm 0.0004$ nm, and for the CoCrFeMnNi alloy, it was $0.3574 \pm 0.0004$ nm.

The X-ray diffraction patterns of the alloys after irradiation with helium ions (Figs. 3 and 4) did not reveal new diffraction peaks or the disappearance of existing ones; that is, no decomposition of solid solutions occurred; therefore, the HEA phase composition is resistant to irradiation. Only the appearance of additional reflections at smaller $\theta$, superimposed on the existing diffraction peaks, leads to the observed asymmetry of the peaks and a shift of the diffraction peaks towards lower values of $\theta$. The asymmetry of the peaks is associated with a change in the lattice parameter of solid solutions with depth as a result of irradiation with helium ions. The shift of the peaks corresponds to an increase in the grating period by $(0.22 \pm 0.01)\%$ for the CoCrFeNi alloy and $(0.11 \pm 0.01)\%$ for the CoCrFeMnNi alloy compared to the nonirradiated alloys.

Bar graphs of the macrostress and microstress values in the nonirradiated and irradiated samples, calculated by the $\sin^2\psi$ method for the (111) orientation and by the Hall method, are shown in Figs. 5 and 6.

According to the data obtained, the tensile stress induced by cold rolling during HEA formation predominates in nonirradiated samples. The level of mac-

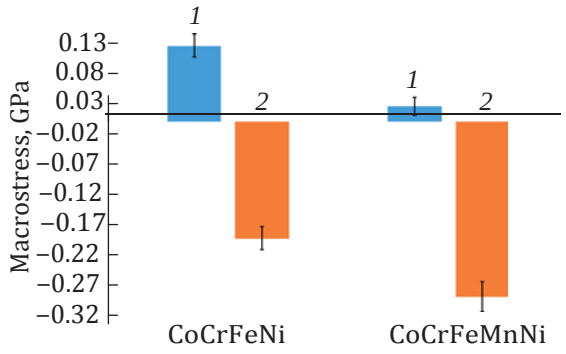


**Fig. 5.** Macrostress diagram in the samples of CoCrFeNi and CoCrFeMnNi alloys (*1*) not irradiated and (*2*) irradiated with $He^{2+}$ ions (40 keV, $2 \times 10^{17}$ $cm^{-2}$).

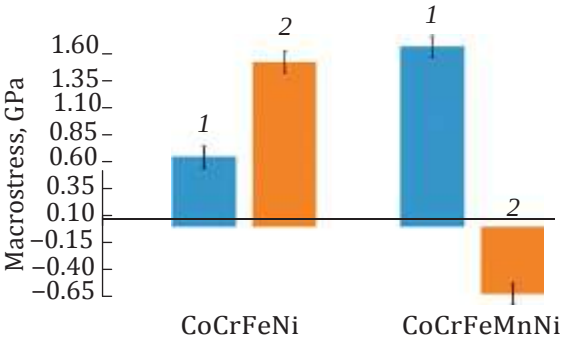


**Fig. 6.** Macrostress diagram in samples of CoCrFeNi and CoCrFeMnNi alloys (*1*) not irradiated and (2) irradiated with $He^{2+}$ ions (40 keV, $2 \times 10^{17}$ $cm^{-2}$).

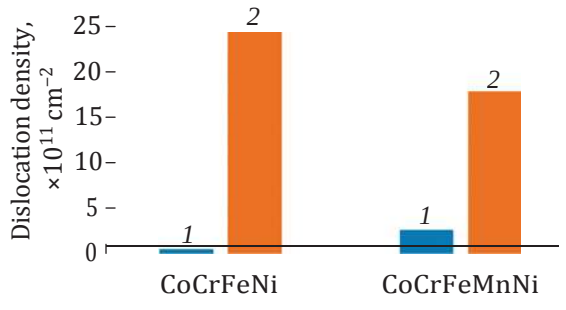


**Fig. 7.** Dislocation density diagram in samples of CoCrFeNi and CoCrFeMnNi alloys (*1*) not irradiated and (2) irradiated with $He^{2+}$ ions (40 keV, $2 \times 10^{17}$ $cm^{-2}$).

rostresses does not exceed 130 MPa, and the level of microstresses is up to 1.67 GPa.

After irradiation with helium ions, the alloys show compressive macrostresses at a level not exceeding 288 MPa (Fig. 5). However, tensile microstresses increase for the CoCrFeNi alloy, and compressive microstresses are observed for the CoCrFeMnNi alloy (Fig. 6).

The Hall method was also used to estimate the sizes of coherent-scattering regions in CoCrFeNi and CoCrFeMnNi alloys; the dislocation density in these alloys was also estimated using the model of dislocation boundaries of coherentscattering regions. The results of estimating the dislocation density in the CoCrFeNi and CoCrFeMnNi HEAs (Fig. 7) suggest that the irradiation of alloys with helium ions leads to a significant increase in the dislocation density in them.

## DISCUSSION

The elemental composition, phase composition, and structure of the CoCrFeNi and CoCrFeMnNi HEAs under consideration are resistant to irradiation with helium ions (40 keV, $2 \times 10^{17}$ $cm^{-2}$); no formation of new phases or surface erosion were found. Thus, the main changes resulting from the irradiation of samples are associated with the formation and interaction of point defects, as well as the formation and redistribution of stress in alloys.

It was found that tensile macrostresses were present in the nonirradiated samples, probably introduced by compression during the cold-rolling stage. After irradiation, under the action of radiation-induced defects and the formation of helium bubbles caused by the implantation of helium ions, compressive macrostresses are formed.

In the process of irradiation with helium ions, vacancies, interstitial atoms, clusters of helium atoms, and vacancies (helium-vacancy) appear in the alloys. As the irradiation dose increases, clusters form nanoscale helium bubbles, and further irradiation leads to an increase in the distribution density and size of these bubbles. The formation of vacancies promotes an increase in the level of tensile microstresses, and the formation of interstitial atoms, interstitial dislocations, and helium bubbles promotes compressive microstresses. HEAs are characterized by suppression of the diffusion of radiation-induced defects, leading to their partial destruction, resulting in the formation of bubbles with a high helium distribution density and small size in comparison with other materials irradiated under similar conditions [1, 17, 22]. In our case, the formation of helium bubbles increases the level of compressive stresses in the HEAs. The relative change in the stress level for CoCrFeNi and CoCrFeMnNi alloys is the same (Fig. 6). However, the different behavior of microstresses during irradiation indicates that in the CoCrFeNi alloy, vacancies have a greater effect on defect formation, and in the CoCrFeMnNi alloy, the formation of helium-vacancy clusters and bubbles predominates.

Some criterion for the radiation resistance of CoCrFeNi and CoCrFeMnNi HEAs, that is, how effectively the alloy suppresses the formation of radiation defects, can be determined from a comparison of the dislocation density (Fig. 7). For the CoCrFeMnNi alloy, a smaller increase in the dislocation density was revealed compared to the CoCrFeNi alloy, which, along with a larger relative increase in the lattice period than for CoCrFeMnNi, indicates a greater resistance of the CoCrFeMnNi HEA to radiation-defect formation.

## CONCLUSIONS

Bulk alloys based on single-phase solid solutions (Co,Cr,Fe,Ni) and (Co,Cr,Fe,Mn,Ni) with a fcc lattice, coarse-grained structure, and homogeneous distribution of elements over the surface and depth were obtained by arc melting under argon, followed by annealing and cold rolling. Twinning and tensile microstresses and macrostresses were observed in the alloys, the appearance of which is associated with the mechanical processing of materials at the manufacturing stage.

The irradiation of HEAs with $He^{2+}$ ions with an energy of 40 keV at a f luence of $2 \times 10^{17}$ $cm^{-2}$ does not change the elemental or phase composition and does not lead to erosion of the surface of the samples. In alloys, the dislocation density increases, which leads to a decrease in the size of coherent-scattering regions, and helium bubbles are also formed, leading to an increase in compressive macrostresses. Tensile microstresses prevail in irradiated CoCrFeNi alloys, while compressive stresses prevail in CoCrFeMnNi alloys.

High-entropy CoCrFeMnNi alloys with a more complex composition are more resistant to radiation damage.

## FUNDING

The study was supported within the framework of the State Scientific Research Program “Energy and Nuclear Processes and Technologies” of the Republic of Belarus (subprogram “Energy Processes and Technologies”, task 2.1.03.2 “Heat-Resistant High-Entropy Alloys Resistant to Extreme Energy Impacts”) and the Science Committee of the Ministry of Education and Science of the Republic of Kazakhstan (grant no. AR14872199).

## CONFLICT OF INTEREST

We declare that we have no conflicts of interest.

## REFERENCES

1. Y. F. Ye, Q. Wang, J. Lu, C. T. Liu, and Y. Yang, Mater. Today **19**, 349 (2016). https://www.doi.org/10.1016/j.mattod.2015.11.026
2. A. M. Manzoni and U. Glatzel, in *Encyclopedia of Materials: Metals and Alloys*, Ed. by F. Caballero (Elesevier, Amsterdam, 2021), **Vol. 2**, p. 441. https://www.doi.org/10.1016/B978-0-12-803581-8.11774-6
3. W. Li, D. Xie, D. Li, Y. Zhang, Y. Gao, and P. K. Liaw, Prog. Mater. Sci. **118**, 100777 (2021). https://www.doi.org/10.1016/j.pmatsci.2021.100777
4. S. Son, S. Kim, J. Kwak, G. H. Gu, D. S. Hwang, Y. T. Kim, and H. S. Kim, Mater. Lett. **300**, 130130 (2021). https://www.doi.org/10.1016/j.jmrt.2022.01.141
5. P. F. Yu, L. J. Zhang, H. Cheng, H. Zhang, M. Z. Ma, Y. C. Li, G. Li, P. K. Liaw, and R. P. Liu, Intermetallics **70**, 82 (2016). https://www.doi.org/10.1016/j.intermet.2015.11.005
6. N. E. Koval, J. I. Juaristi, R. D. Muino, and M. Alducin, J. Appl. Phys. **127**, 145102 (2020). https://www.doi.org/10.1063/1.5142239
7. Y. Zhang, T. T. Zuo, Z. Tang, M. C. Gao, K. A. Dahmen, P. K. Liaw, and Z. P. Lu, Prog. Mater. Sci. **6**, 1 (2014). https://www.doi.org/10.1016/j.pmatsci.2013.10.001
8. B. Cantor, I. T. H. Chang, P. Knight, and A. J. B. Vincent, Mater. Sci. Eng., A **375–377**, 213 (2020). https://www.doi.org/10.1016/j.msea.2003.10.257
9. O. N. Senkov, J. M. Scott, S. V. Senkova, D. B. Miracle, C. F. Woodward, J. Alloys Compd. **609**, 6043 (2011). https://www.doi.org/10.1016/j.jallcom.2011.02.171
10. A. Karati, K. Guruvidyathri, V. S. Hariharan, and B. S. Murty, Scr. Mater. **162**, 465 (2019). https://www.doi.org/10.1016/j.scriptamat.2018.12.017
11. V. Pacheco, G. Lindwall, D. Karlsson, J. Cedervall, S. Fritze, G. Ek, P. Berastegui, M. Sahlberg, and U. Jansson, Inorg. Chem. **58**, 811 (2019). https://www.doi.org/10.1021/acs.inorgchem.8b02957
12. S. Q. Xia, Z. Wang, T. Yang, and Y. Zhang, J. Iron Steel Res. **22**, 879 (2015). https://www.doi.org/10.1016/S1006-706X(15)30084-4
13. N. G. Jones and L. R. Owen, in *Encyclopedia of Materials: Metals and Alloys*, Ed. by F. Caballero (Elesevier, Amsterdam, 2021), **Vol. 2**, p. 393. https://www.doi.org/10.1016/B978-0-12-803581-8.12124-1
14. Y. Tian, L. Li, J. Li, Y. Yang, S. Li, and G. Qin, Adv. Eng. Mater. **23**, 2001514 (2021). https://www.doi.org/10.1002/adem.202001514
15. Y. Lu, H. Huang, X. Gao, C. Ren, J. Gao, H. Zhang, S. Zheng, Q. Jin, Y. Zhao, L. Chenyang, T. Wang, and T. Li, J. Mater. Sci. Technol. **35**, 369 (2018). https://www.doi.org/10.1016/j.jmst.2018.09.034

16. H. Song, Q. Ma, W. Zhang, and F. Tian, J. Alloys Compd. **885**, 160944 (2021). https://www.doi.org/10.1016/j.jallcom.2021.160944

17. Z. Zhang, E. H. Han, and C. Xiang, Corros. Sci. **191**, 109742 (2021). https://www.doi.org/10.1016/j.corsci.2021.109742

18. B. S. Murty, J.-W. Yeh, and S. Ranganathan, *High-Entropy Alloy* (Butterworth-Heinemann, Oxford, 2014).

19. C. Lee, Y. Chou, G. Kim, G. Song, M. C. Gao, C. Zhang, W. Chen, J. Poplawsky, Y. C. Chou, H. Choo, and P. K. Liaw, Adv. Mater. **32**, 2004029 (2020). https://www.doi.org/10.1002/adma.202004029

20. A. S. Rogachev, Phys. Met. Metallogr. **121**, 733 (2020). https://doi.org/10.1134/S0031918X20080098

21. SRIM. http://www.srim.org/.

22. Z. Zhang, D. E. J. Armstrong, and P. S. Grant, Prog. Mater. Sci. **123**, 100807 (2022). https://www.doi.org/10.1016/j.pmatsci.2021.100807

*Translated by O. Zhukova*

SPELL: 1. OK